Low-dimensional state-space representations for classical unsteady aerodynamic models

Steven L. Brunton*, Clarence W. Rowley†
Princeton University, Princeton, NJ 08544

This work develops reduced-order models for the unsteady aerodynamic forces on a small wing in response to agile maneuvers and gusts. In particular, the classical unsteady models of Wagner[1] and Theodorsen[2] are cast into a low-dimensional, state-space framework. Low order state-space models are more computationally efficient than the classical formulations, they may be naturally incorporated to the design of flight controllers, and may be extended to include nonlinearities. A method to empirically tune Theodorsen's model and cast it into state-space form is presented. Reduced order models linearized at various angles of attack, from $\alpha = 0^\circ$ to $\alpha = 25^\circ$, are obtained from the indicial response using the eigensystem realization algorithm.[3–6] The behavior and performance of the models are investigated in the frequency domain, and by testing on a rapid pitch maneuver with large angle of attack. Direct numerical simulations are performed using an immersed boundary projection method[7,8] for a flat plate at Reynolds number 100.

Nomenclature

α	Angle of attack of airfoil
c	Chord length of airfoil
b	Half-chord of airfoil
U_∞	Free stream velocity
a	Pitch axis location with respect to $1/2-$chord ($a=-1$ leading edge, $a=1$ trailing edge)
x/c	Pitch axis location with respect to chord ($x/c=0$ leading edge, $x/c=1$ trailing edge)
L	Lift force
$C_L = 2L/\rho U_\infty^2 c$	Lift coefficient
$k = \omega c/2U_\infty$	Reduced frequency, non-dimensionalized by chord c
$C(k)$	Theodorsen's function
(A_r, B_r, C_r, D_r)	Reduced order ERA model of order r
C_{L_α}	Lift coefficient slope in angle of attack α

I. Introduction

Most aerodynamic models used for flight control rely on the quasi-steady assumption that lift and drag forces depend in a static manner on parameters such as relative velocity and angle of attack. While these models work well for conventional aircraft,[9] they do not describe the unsteady aerodynamic forces that become increasingly important for small, agile aircraft. The unsteady flow over small-scale wings has gained significant attention recently, both to study bird and insect flight as well as to develop advanced aerodynamic models for high-performance micro-aerial vehicles (MAVs). The short time scales involved in gusts and agile maneuvering makes small wings susceptible to unsteady laminar separtion, which can either enhance or destroy the lift depending on the specific maneuver. For example, certain insects[10–12] and birds[13] use the shape and motion of their wings to maintaing the high transient lift associated with a rapid pitch-up, while

*Graduate Student, Mechanical and Aerospace Engineering, Student Member, AIAA.
†Associate Professor, Mechanical and Aerospace Engineering, Associate Fellow, AIAA.

avoiding stall and the substantially decreased lift which follows. Moreover, at smaller size scales, added-mass forces become increasingly important. The potential performance gains observed in bio-locomotion make this an interesting problem for model-based control in the arena of MAVs.[14] For a good overview of the effect of Reynolds number and aspect ratio on small wings, see Ol *et al.*[15,16]

The unsteady models of Wagner[1] and Theodorsen[2] are widely used,[17] and they have shown better agreement with simulations than quasi-steady models for a large range of Strouhal numbers and reduced frequencies for pitching and plunging flat plate airfoils.[18,19] A hierarchy of models based on Wagner's and Theodorsen's classical methods, but extended to include nonlinear separated flow effects, such dynamic stall[20–22] and vortex shedding,[19,23] is ideal for capturing the effects of agile maneuvers and gusts on small-scale wings. However, both Wagner's and Theodorsen's methods are formulated using mathematical machinery that limit their usefulness. In particular, Wagner's indicial response method is based on the convolution integral, and Theodorsen's model uses a transfer function $C(k)$ which is not a rational function; as a consequence, neither of these models is directly suitable for flight control design.

In order to develop controllers suitable for unsteady aerodynamics, it is essential to have a framework of models which are both physically accurate and computationally tractable. Low order state-space models are ideal for control design because they fit naturally into existing flight dynamic models. Previous work[5,6] developed tools to cast Wagner's indicial response in terms of a low-dimensional, state-space model using the eigensystem realization algorithm (ERA).[3] It has recently been shown[4] that ERA produces the same reduced order models (ROMs) as the method of snapshot-based balanced proper orthogonal decomposition (BPOD),[24] without the need for adjoint simulations. The resulting ROMs are ideal for fast, flexible computation, modification with nonlinear dynamics and the application of control techniques.

Theodorsen's model and Wagner's indicial response, as originally formulated, are linearized about $\alpha = 0$. However, the lift coefficient depends nonlinearly on angle of attack as seen in Figure 1. At Reynold's number Re= 100, the flow past a flat plate at angle of attack α has been shown to undergo a Hopf bifurcation at $\alpha_{\text{crit}} \approx 28°$, the critical angle of attack.[14] Before the critical angle, the flow field is steady, and after the critical angle, the flow is characterized by periodic vortex shedding. The average lift in the case of vortex shedding is significantly higher than the lift of the unstable steady state. During rapid, large amplitude pitch-up, the flow may separate at the leading edge, trailing edge, or both. A canonical maneuver of particular interest involves a rapid pitch-up, followed by a pause and a pitch-down,[25,26] which is characterized by the formation and convection of a large leading edge vortex (LEV).[10,13,14,27]

The following work develops a method for empirically tuning Theodorsen's model and casting it into state-space form. In addition, to better capture the dynamics near stall, we investigate generalized indicial response models that are linearized about larger angles of attack, $\alpha \in [0°, 25°]$.

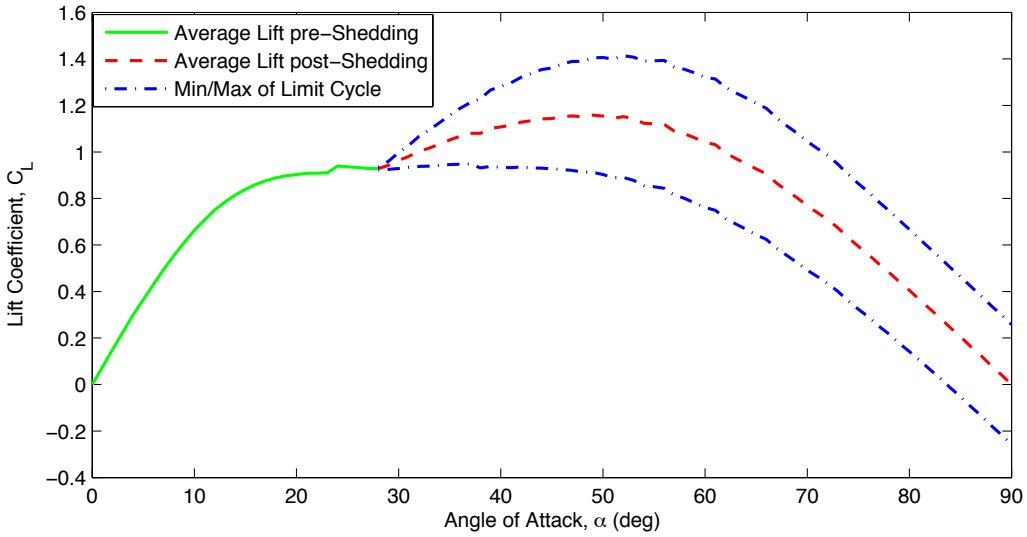

Figure 1. Lift coefficient vs. angle of attack for a flat plate at $Re = 100$. A Hopf bifurcation occurs at $\alpha \approx 28°$, resulting in unsteady periodic vortex shedding.

II. Empirical Theodorsen model

To model the aerodynamic forces acting on an airfoil in motion, it is natural to start with a quasi-steady approximation. Thin airfoil theory assumes that the airfoil's vertical center of mass h and angle of attack α motion is relatively slow and small, so that the flow field locally equilibrates to the motion. Thus, $\dot{h}$ and $\dot{\alpha}$ effects may be explained by effective angle of attack and effective camber, respectively:

$$C_L = 2\pi\left(\alpha + \dot{h} + \frac{1}{2}\dot{\alpha}\left(\frac{1}{2} - a\right)\right) \tag{1}$$

Lengths have been nondimensionalized by c and time is nondimensionalized by c/U_∞, where U_∞ is the free stream velocity, c is the chord length and a is the pitch axis location with respect to the $1/2-$chord (e.g., pitching about the leading edge corresponds to $a = -1$, whereas the trailing edge is $a = 1$).

For more rapid maneuvers, it is necessary to include added-mass terms which account for the reaction force due to the mass of fluid which is accelerated directly by the airfoil. Theodorsen's frequency domain model[2,17] includes the additional added-mass terms and multiplies the circulatory lift from thin airfoil theory by Theodorsen's transfer function $C(k)$, relating sinusoidal inputs of reduced frequency[28] $k = \omega c/2U_\infty$ to their aerodynamic response.

$$C_L = \underbrace{\frac{\pi}{2}\left[\ddot{h} + \dot{\alpha} - \frac{a}{2}\ddot{\alpha}\right]}_{\text{Added-Mass}} + \underbrace{2\pi\left[\alpha + \dot{h} + \frac{1}{2}\dot{\alpha}\left(\frac{1}{2} - a\right)\right]}_{\text{Circulatory}} C(k) \tag{2}$$

$C(k)$ is expressed in terms of Hankel functions in the following way:

$$C(k) = \frac{H_1^{(2)}(k)}{H_1^{(2)}(k) + iH_0^{(2)}(k)} \tag{3}$$

where $H_\nu^{(2)} = J_\nu - iY_\nu$, and J_ν and Y_ν are Bessel functions of the first and second kind, respectively. When length and time are nondimensionalized so $c = U_\infty = 1$, the reduced frequency k is related to the frequency of motion by $k = w/2$.

A. Rewriting equations

Here we only consider pitching motion. It is possible to improve Theodorsen's model by replacing the coefficients $\pi/2$ and 2π, which are obtained using linearized potential flow theory, with generalized coefficients C_1 and C_2. The new coefficients may be obtained empirically, either through simulation or experiment, at a given Reynolds number and wing geometry. This yields better performance in the limit of low and high frequency motions. Eq. (2) for pitching becomes:

$$C_L = C_1\left[\dot{\alpha} - \frac{a}{2}\ddot{\alpha}\right] + C_2\left[\alpha + \frac{1}{2}\dot{\alpha}\left(\frac{1}{2} - a\right)\right] C(k). \tag{4}$$

If the input is $u = \ddot{\alpha}$ and the output is $y = C_L$, Theodorsen's model yields the following transfer function:

$$\frac{\mathcal{L}[C_L]}{\mathcal{L}[\ddot{\alpha}]} = C_1\left(\frac{1}{s} - \frac{a}{2}\right) + C_2\left[\frac{1}{s^2} + \frac{1}{2s}\left(\frac{1}{2} - a\right)\right] C(s) \tag{5}$$

where $C(s)$ is Theodorsen's transfer function, and $s = 2k$ is the Laplace variable, which is twice the reduced frequency if $c = U_\infty = 1$. Eq. (5) is represented schematically in Figure 2.

Finally, we know that Theodorsen's function $C(k)$ is 1 at low frequencies and $1/2$ at high frequencies. Therefore, it is convenient to decompose $C(k) = 1 - C'(k)$. This results in the following model:

$$C_L = \underbrace{-\frac{a}{2}C_1}_{C_{L_{\ddot{\alpha}}}}\ddot{\alpha} + \underbrace{\left[C_1 + \frac{C_2}{2}\left(\frac{1}{2} - a\right)\right]}_{C_{L_{\dot{\alpha}}}}\dot{\alpha} + \underbrace{C_2}_{C_{L_\alpha}}\alpha - \underbrace{C_2 C'(k)\left[\alpha + \frac{1}{2}\dot{\alpha}\left(\frac{1}{2} - a\right)\right]}_{\text{fast dynamics}} \tag{6}$$

Equating the coefficient of the $\ddot{\alpha}$ and α terms in Eqs. (4) and (14) results in expressions for the coefficients in terms of stability derivatives: $C_1 = -2C_{L_{\ddot{\alpha}}}/a$ and $C_2 = C_{L_\alpha}$. There are a number of ways to handle the fast dynamics. The simplest approach involves using Theodorsens function $C(k) = 1 - C'(k)$. It may also be possible to approximate this term using a system ID approach. We may also approximate Theodorsen's function using a Padé approximation.

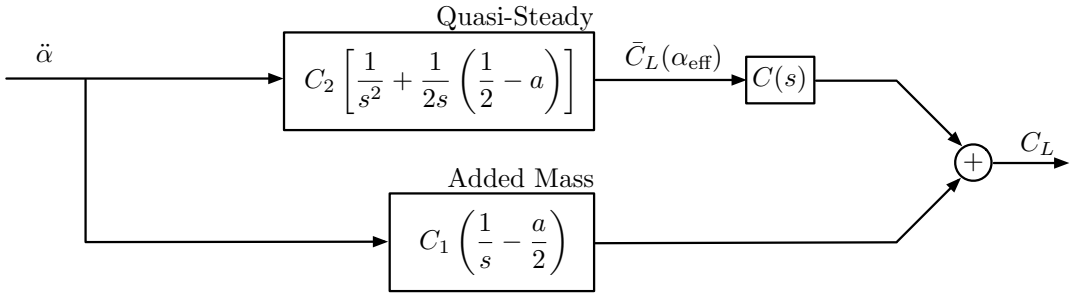

Figure 2. Schematic for empirical Theodorsen's model, Eq. (5), for a pitching airfoil.

B. Empirical Theodorsen function $C(k)$

A Padé approximation of Theodorsen's transfer function was used to develop ROMs for the effect of synthetic jet actuators on the forces and moments on an airfoil.[29] The approximation is given by the following:

$$C(k) \approx .99612 - .1666\frac{k}{k+.0553} - .3119\frac{k}{k+.28606} \tag{7}$$

$$\approx \frac{.5177k^2 + .2752k + .01576}{k^2 + .3414k + .01582} \tag{8}$$

In the Laplace variable $s = 2k$, this becomes:

$$C(s) \approx \frac{.1294s^2 + .1376s + .01576}{.25s^2 + .1707s + .01582} \tag{9}$$

Although the approximation does not perfectly reproduce $C(s)$, the overall effect on Theodorsen's lift model is negligible, as shown in Figure 3.

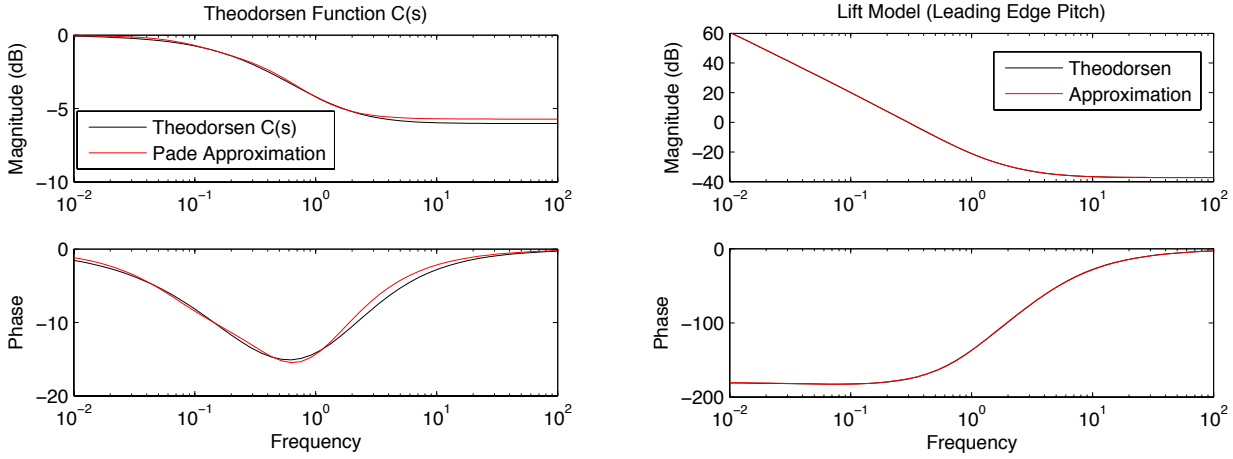

Figure 3. (Left) Theodorsen's transfer function $C(s)$ (black) and its Padé approximation (red). (Right) Resulting lift model for leading-edge pitching, Eq. (2), with $\ddot{\alpha}$ as input and C_L as output.

Alternatively, we may start with a ROM based on the indicial response.[6] Subtracting off the added-mass terms and dividing through by the quasi-steady terms results in an empirical $C(s)$, shown in Figure 4.

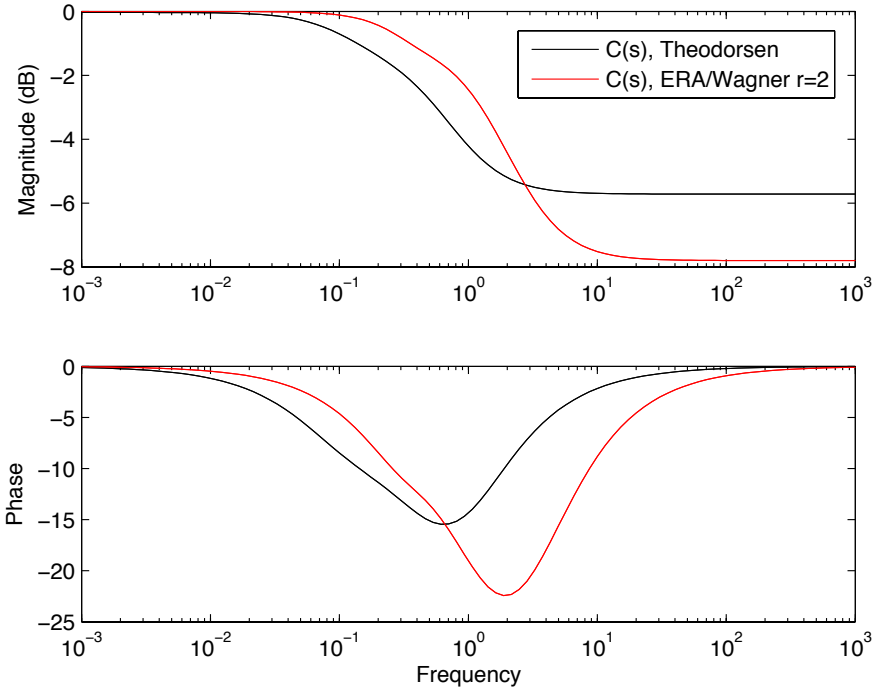

Figure 4. Theodorsen's transfer function $C(s)$ from theory (black) and backed out of ERA model (red).

C. State-space representation

A state-space representation of Theodorsen's model is desirable for simulating in the time-domain as well as for the application of modern control techniques. To obtain such a representation, we use the schematic in Figure 2 of Eq. (5), as well as the Padé approximation of $C(s)$ from Eq.(9). In particular, we may readily obtain minimal state-space representations of each of the blocks in Figure 2, and combine the models using standard block diagram algebra. This results in the following minimal representation:

$$\frac{d}{dt}\begin{bmatrix} x_1 \\ x_2 \\ \alpha \\ \dot{\alpha} \end{bmatrix} = \begin{bmatrix} -.6828 & -.0633 & C_2 & C_2(1-2a)/4 \\ 1 & 0 & 0 & 0 \\ 0 & 0 & 0 & 1 \\ 0 & 0 & 0 & 0 \end{bmatrix} \begin{bmatrix} x_1 \\ x_2 \\ \alpha \\ \dot{\alpha} \end{bmatrix} + \begin{bmatrix} 0 \\ 0 \\ 0 \\ 1 \end{bmatrix} \ddot{\alpha} \tag{10}$$

$$C_L = \begin{bmatrix} .197 & .0303 & .5176C_2 & C_1 + .5176C_2(1-2a)/4 \end{bmatrix} \begin{bmatrix} x_1 \\ x_2 \\ \alpha \\ \dot{\alpha} \end{bmatrix} - \frac{aC_1}{2}\ddot{\alpha} \tag{11}$$

where C_1 and C_2 are the empirically determined coefficients from above, and x_1 and x_2 are states necessary to model $C(s)$.

D. Frequency domain analysis

Equipped with a tractable form of Theodorsen's model, it is possible to investigate the effect of varying the pitch point. In Figure 5, we plot the frequency response of Theodorsen's model, with input $\ddot{\alpha}$ and output C_L, as the pitch point varies from leading edge ($x/c = 0$, $a = -1$) to the trailing edge ($x/c = 1$,$a = 1$). We see a qualitative change as the pitch point is moved aft of the mid-chord, after which the effect of added-mass terms on high frequency motions becomes negative; i.e., the phase approaches $-180°$ for large frequency.

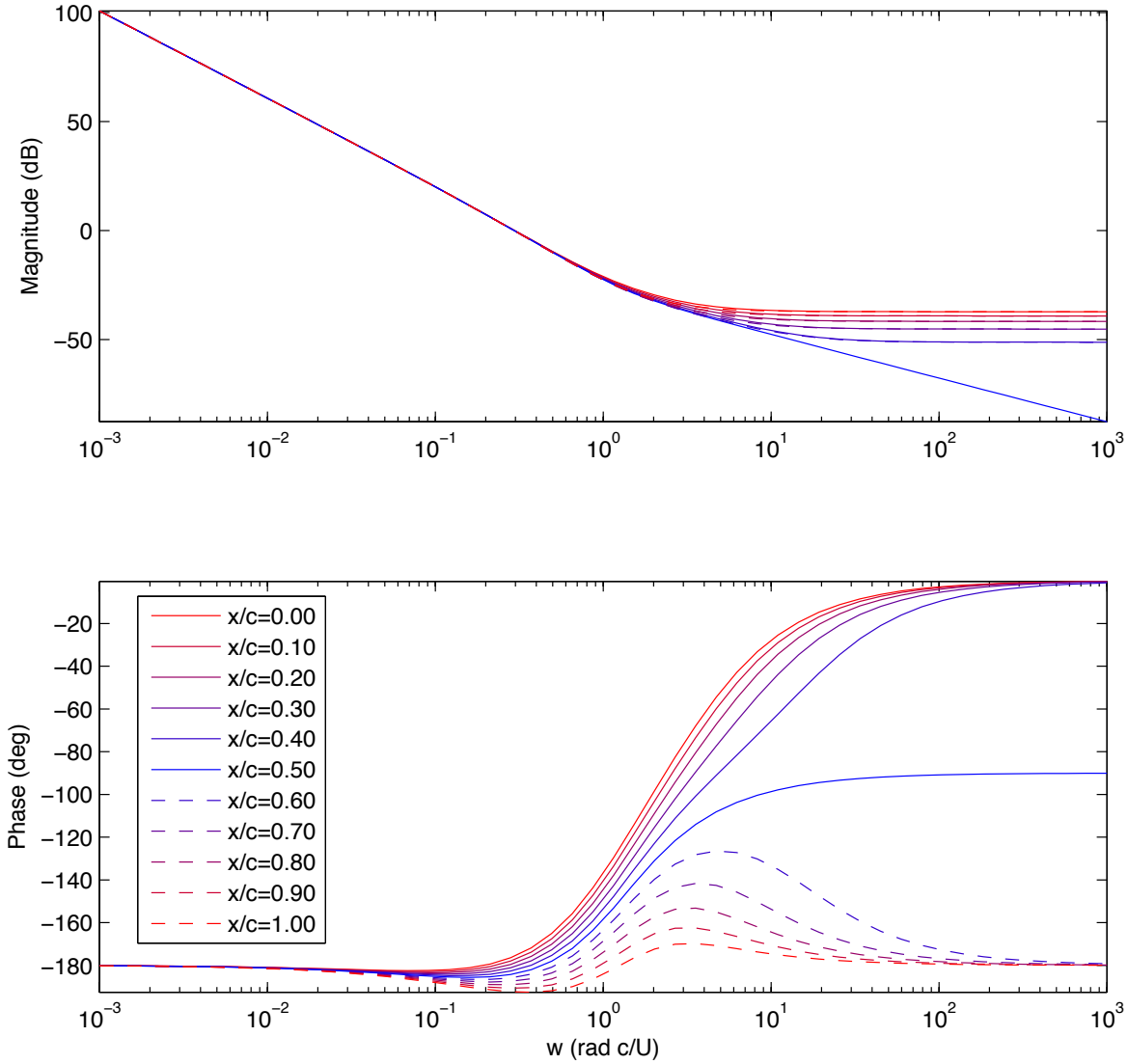

Figure 5. Bode plots of Theodorsen's model for an airfoil pitching at various locations along the chord, from leading edge ($x/c = 0$) to trailing edge ($x/c = 1$). The input is $\ddot{\alpha}$ and output is C_L.

To understand this, we investigate how the poles and zeros of the system change as pitch point is varied. Because the pitch point a only enters into the model, Eq. (5), in the numerator, the poles never change. Figure 6 shows how the zeros move as pitch point is varied. In particular, we see that as the pitch point moves aft of the mid-chord the branch of real zeros exits at negative infinity and re-enters at positive infinity. The appearance of a zero in the right half plane makes the system non-minimum phase. A direct result is that given a positive step in angle of attack, the lift initially moves in the opposite direction, because of negative added-mass forces, before the circulatory forces have a chance to catch up and the system relaxes to a positive steady state.

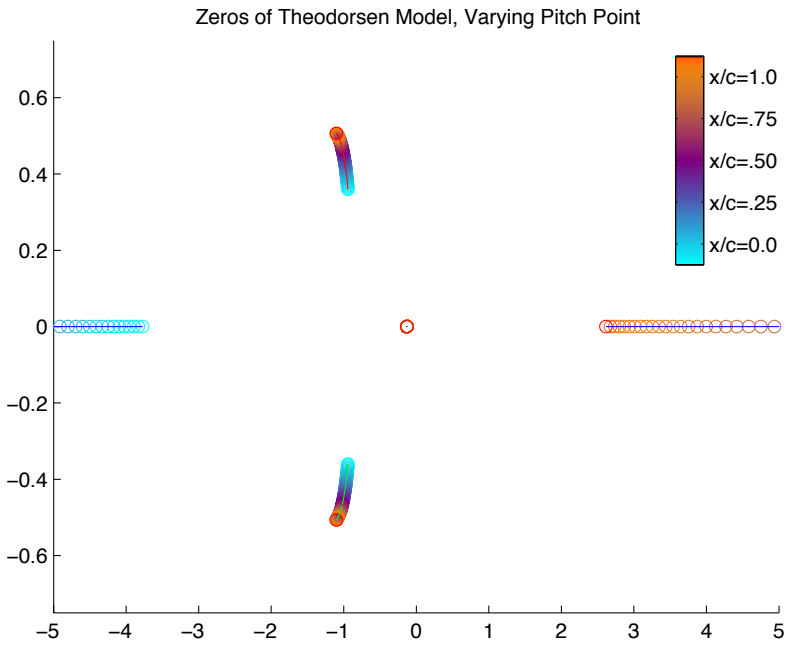

Figure 6. Zeros of Theodorsen's lift model at $\alpha = 0$ as pitch axis moves from the leading edge ($x/c = 0$) to the trailing edge ($x/c = 1$). The zero at $s \approx -4$ for leading-edge pitching ($x/c = 0$) goes to the point at infinity for $x/c = 0.5$, and then reappears as a right-half-plane zero $x/c > 0.5$.

III. Indicial response ROM at non-zero angle of attack

The time domain method of Wagner[1] makes it possible to reconstruct the lift response to an arbitrary motion, in say angle of attack $\alpha(t)$, by superposition of the "indicial" lift response $C_L^S(t)$, defined as the C_L response due to a step in the input variable, $\dot{\alpha} = \delta(t)$:

$$C_L(t) = C_L^S(t)\alpha(0) + \int_0^t C_L^S(t-\tau)\dot{\alpha}(\tau)d\tau \tag{12}$$

Wagner originally derived the indicial response analytically, accounting for added-mass and shed-wake effects in a manor similar to that of Theodorsen. However, it is possible to interpret the method more generally as applying to step-response data obtained from experiments or simulation, reducing the number of simplifying assumptions. Therefore, the only assumption is that of linearity. However, it is clear from Figure 1 that the lift coefficient is only locally linear in angle of attack, so an indicial response model based on a step response from $\alpha = 0^\circ$ to $\alpha = 1^\circ$ may not be accurate for maneuvers with large angle of attack.

A systematic approach has been developed[6] to obtain a reduced order model (ROM) for the indicial response by first subtracting off the added-mass and quasi-steady forces from the step response and modeling the remainder using the eigensystem realization algorithm (ERA). The ROM has the following form:

$$\begin{aligned} \frac{d}{dt}\begin{bmatrix}\mathbf{x}\\ \alpha\\ \dot{\alpha}\end{bmatrix} &= \begin{bmatrix}A_r & 0 & 0\\ 0 & 0 & 1\\ 0 & 0 & 0\end{bmatrix}\begin{bmatrix}\mathbf{x}\\ \alpha\\ \dot{\alpha}\end{bmatrix}_k + \begin{bmatrix}B_r\\ 0\\ 1\end{bmatrix}\ddot{\alpha}_k \\ C_L(t) &= \begin{bmatrix}C_r & C_{L_\alpha} & C_{L_{\dot{\alpha}}}\end{bmatrix}\begin{bmatrix}\mathbf{x}\\ \alpha\\ \dot{\alpha}\end{bmatrix} + C_{L_{\ddot{\alpha}}}\ \ddot{\alpha} \end{aligned} \tag{13}$$

The input is $\ddot{\alpha}$, the output is lift coefficient C_L, and the model structure is conveniently expressed in terms of the stability derivatives, $C_{L_{\alpha_i}} \cdot \alpha_i$, and the additional fast dynamics, $C_r \cdot \mathbf{x}$:

$$C_L = C_{L_\alpha} \cdot \alpha + C_{L_{\dot{\alpha}}} \cdot \dot{\alpha} + C_{L_{\ddot{\alpha}}} \cdot \ddot{\alpha} + C_r \cdot \mathbf{x} \tag{14}$$

It is possible to use this reduced order modeling technique to obtain indicial response ROMs linearized about non-zero angle of attack. First, take an airfoil at non-zero angle of attack, α_0, with a fully developed boundary layer; the lift coefficient $C_L(\alpha_0)$ may be non-zero. Now, obtain the step response starting from this non-zero angle of attack, and obtain a model from the transient $C_L(t) - C_L(\alpha_0)$ using the method above. The output of this model is the lift in excess of $C_L(\alpha_0)$ due to pitching about α_0.

Using this technique, we obtain ROMs for a flat plate at Reynolds number 100 linearized about various angle of attack $\alpha \in [0°, 25°]$. We obtain a ROM at every degree, so there are 26 models.

A. Frequency domain analysis

Using the models computed above, we plot the frequency response of models linearized at $\alpha \in [0°, 25°]$, shown in Figure 7. As seen in Figure 1, the lift slope decreases for increasing angle of attack, so it is not surprising that the magnitude of the low frequency motions decreases for increasing angle of attack. Additionally, we see that at larger angle of attack the phase converges to $-180°$ at much lower frequencies, indicating that solutions take longer to reach equilibrium in the time domain. This is consistent with the fact that for larger angle of attack the system is closer to instability, and a pair of eigenvalues of the system are moving closer to the imaginary axis, effecting the time-scale of relaxation.

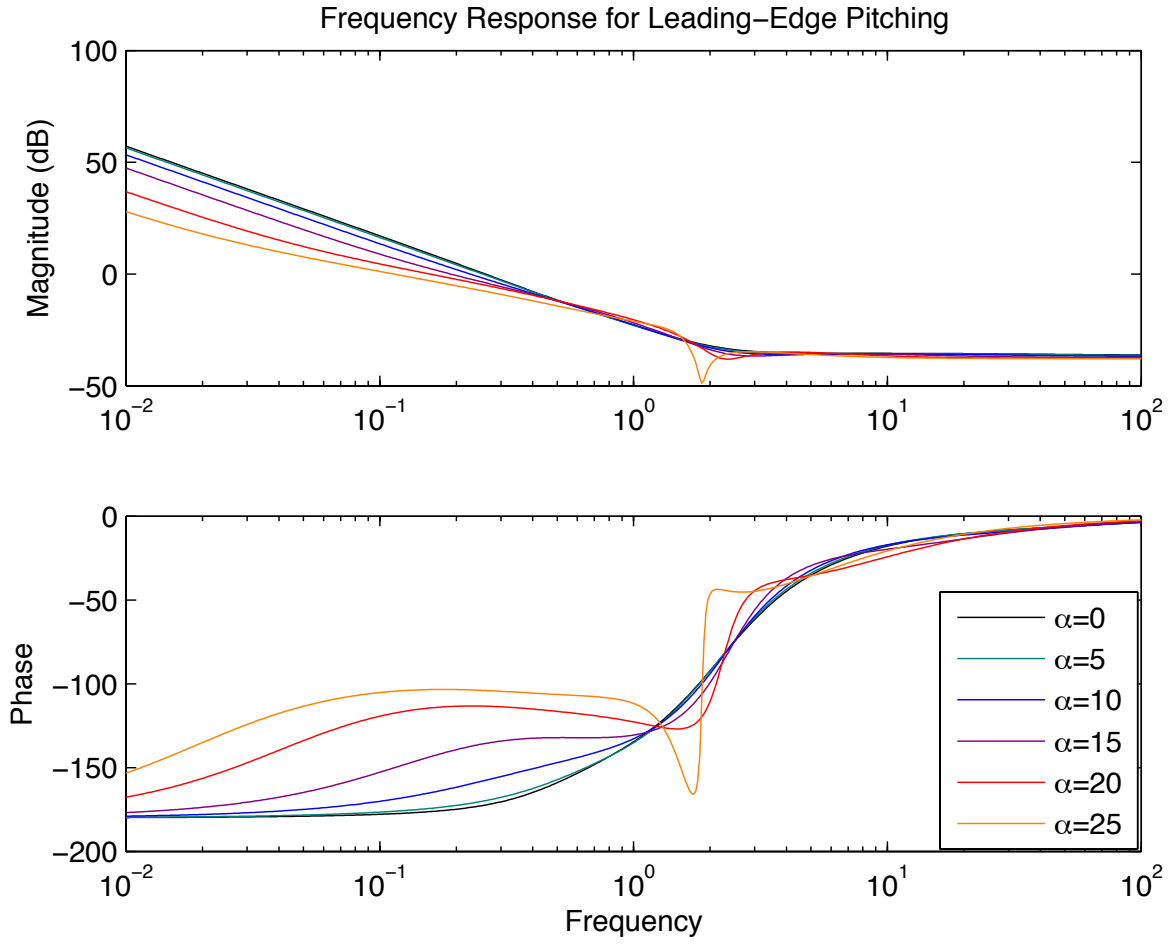

Figure 7. Frequency response of indicial response ROM linearized at various angle of attack, α.

To see this more clearly, we plot the poles and zeros of the ROM for $\alpha \in [0°, 25°]$, shown in Figure 8. The model given by Eq. (13) always has two poles at the origin because the input $\ddot{\alpha}$ must be integrated twice to obtain the states $\dot{\alpha}$ and α. Because we use an ERA model of order $r = 3$ for the fast dynamics, there are an additional three branches of poles, as indicated in the plot. Similarly, there are five branches of zeros. The three branches on or closest to the real axis correspond to the ERA model, while the two nearly circular branches correspond to the integral states.

The most striking feature of Figure 8 is that as angle of attack increases, a pair of poles and a pair of zeros march towards the imaginary axis. This explains the longer relaxation times (convergence of Bode plots to $-180°$ at successively lower frequencies). It also indicates that the ROMs are capturing the dynamics as the system approaches a Hopf bifurcation.

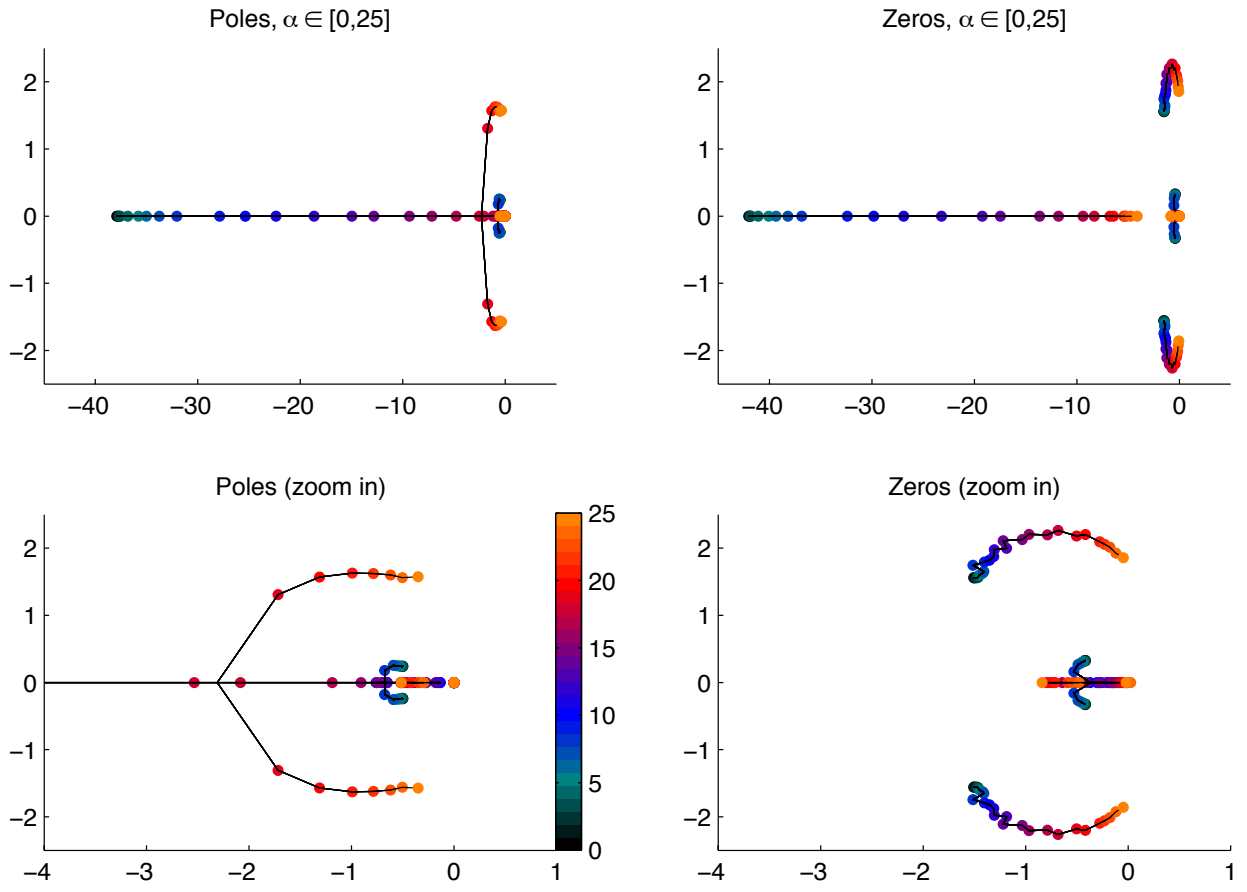

Figure 8. Poles and zeros of indicial response ROM linearized at various angle of attack, from $\alpha = 0°$ (black) to $\alpha = 25°$ (orange).

B. Comparison with DNS

To assess the performance of the indicial response ROMs linearized at non-zero α, we compare the models to direct numerical simulation (DNS) for small and large amplitude motions. The small amplitude motions are $1°$ amplitude sinusoidal motions about a base angle of attack α_0, and the large amplitude motion is a canonical pitch-up, hold, pitch-down maneuver.[26]

Figure 9 shows the frequency response of three ROMs, linearized at $\alpha_0 = 0°$, $\alpha_0 = 10°$, and $\alpha_0 = 20°$, respectively, and the corresponding data from DNS. The agreement between DNS and ROM is not perfect; however, it is clear that the ROM linearized at $\alpha_0 = 20°$ is better captures the small amplitude motions at $\alpha = 20°$ than either of the other two models.

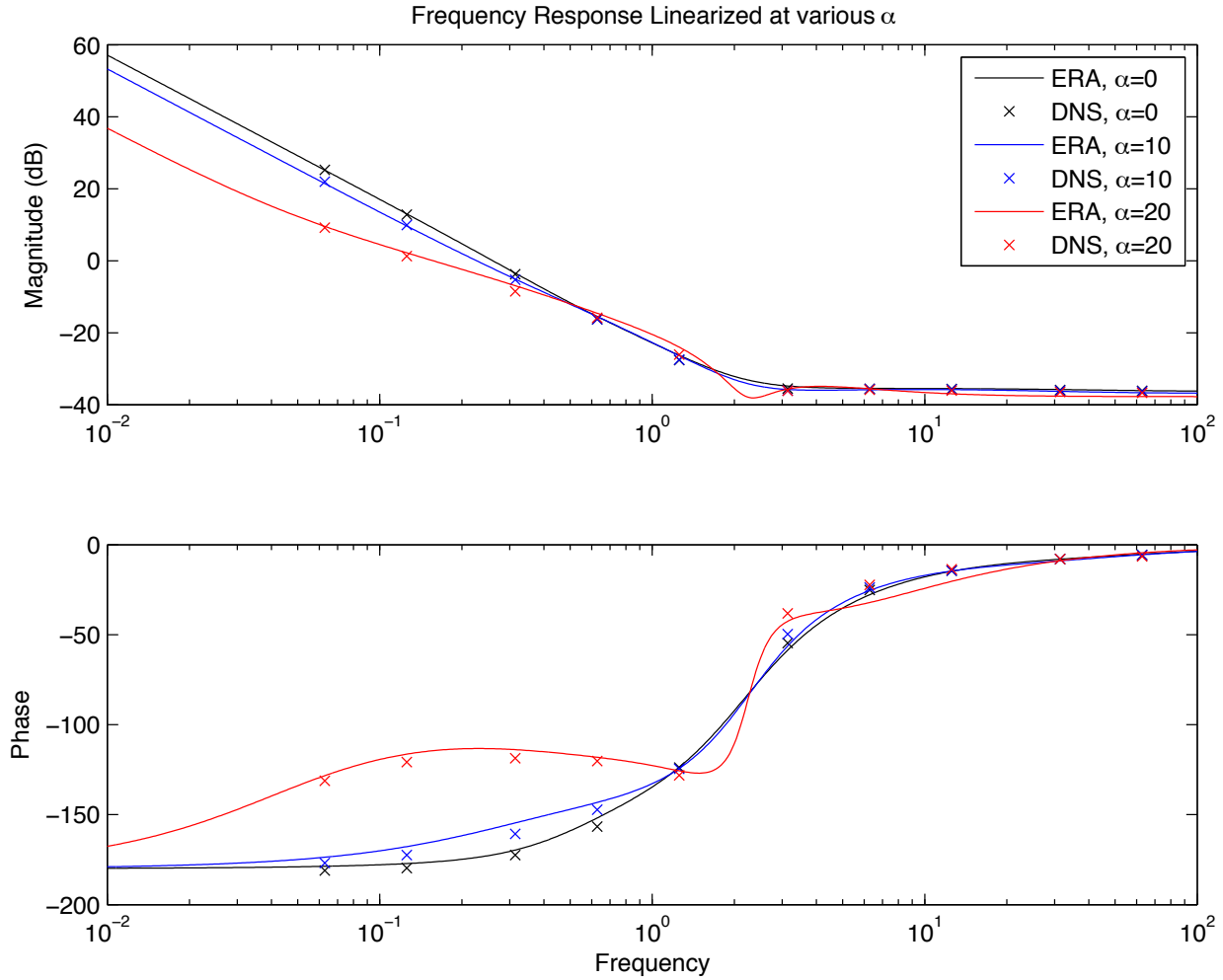

Figure 9. Frequency response of indicial response ROMs linearized at various angle of attack, α, plotted against DNS ($\times$).

The large amplitude motion is a canonical pitch-up, hold, pitch-down maneuver.[26] The pitch maneuver consists of a pitch-up, hold, pitch-down about the leading edge with an angle of attack starting at 15° and reaching a maximum angle of 25°. This specific maneuver is chosen because of its relationship to the canonical test case[26] and because it involves large added-mass forces and leading-edge separation. The motion is given by the following expression:

$$G(t) = \log\left[\frac{\cosh(a(t-t_1))\cosh(a(t-t_4))}{\cosh(a(t-t_2))\cosh(a(t-t_3))}\right] \qquad \alpha(t) = \alpha_0 + \alpha_{\max}\frac{G(t)}{\max(G(t))} \tag{15}$$

where $a = 11$, $\alpha_0 = 15°$ and $\alpha_{\max} = 10°$. For the pitching motion, $t_1 = 1, t_2 = 3, t_3 = 4, t_4 = 6$.

Figure 10 shows the performance of a ROM linearized at $\alpha_0 = 0°$ and a ROM linearized at $\alpha_0 = 15°$ on the large amplitude maneuver. The top plot is the maneuver itself, and the bottom plot shows the lift coefficient of each model throughout the maneuver. It is clear that the model linearized at $\alpha_0 = 15°$ outperforms the model linearized at $\alpha_0 = 0°$. This is not surprising, considering that the maneuver starts at 15°. It is somewhat surprising, however, that the second model is able to capture the lift curve, considering the strongly separated flow.

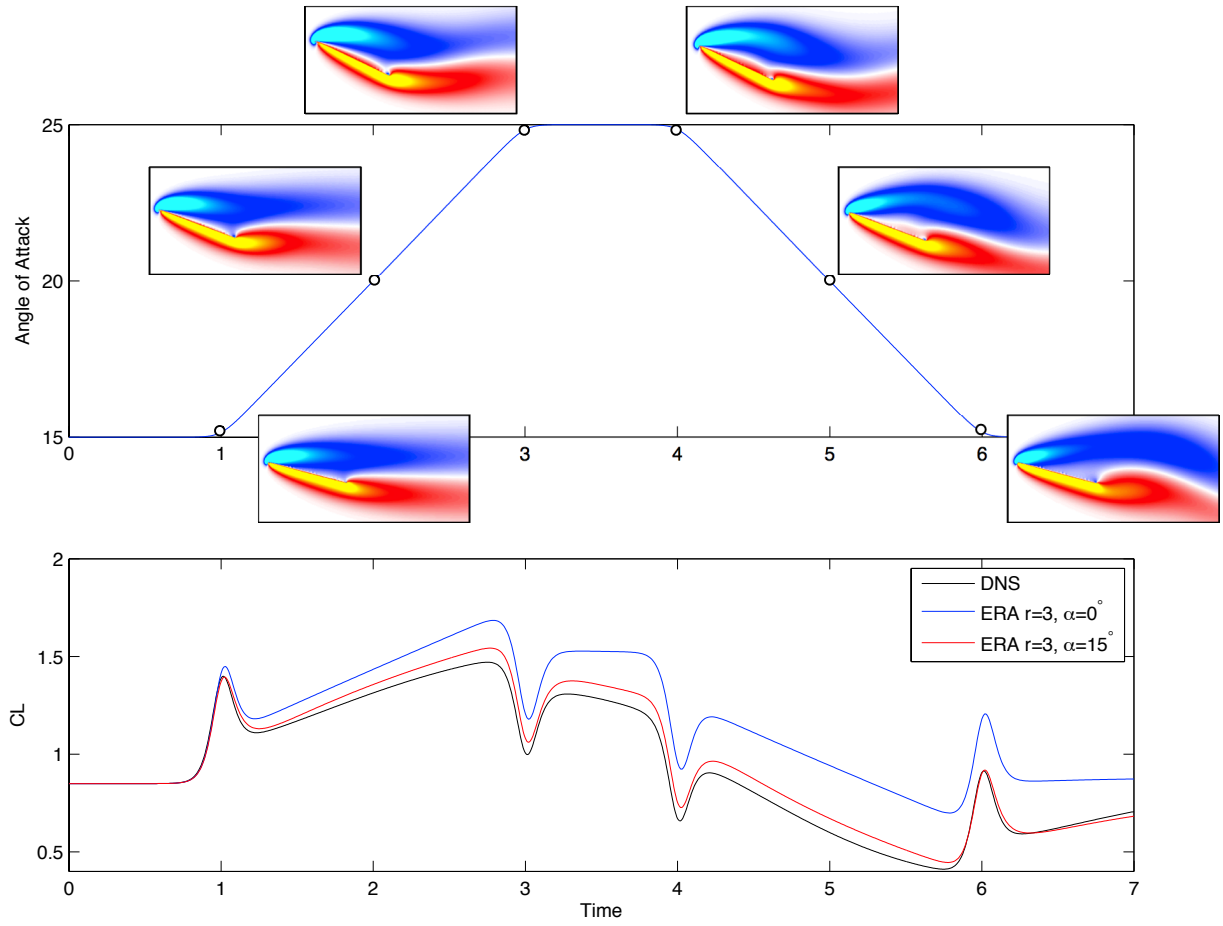

Figure 10. Comparison of indicial response ROMs linearized about $\alpha = 0$ and $\alpha = 15$ against DNS for canonical pitch-up, hold, pitch-down maneuver from 15° to 25°. Vorticity fields are plotted showing the formation and shedding of a weak leading edge vortex (LEV).

IV. Conclusions

This work has developed low-dimensional, state-space representations of the classical unsteady aerodynamic models of Wagner and Theodorsen.

By using a Padé approximation for Theodorsen's function $C(s)$,[29] we have obtained rational transfer function and corresponding minimal state-space representations for Theodorsen's lift model. Additionally, it is possible to tune the lift coefficient slopes for the added-mass and quasi-steady terms using empirical data. This guarantees agreement of the model in the limit of high and low frequency motions. Finally, it is possible to obtain an empirical $C(s)$ from a reduced-order model determined from an indicial response.

A state-space representation for Theodorsen's lift model has many immediate benefits, including compatibility with optimal control[29] and analysis techniques. In our analysis, we have investigated the frequency response of the system as the pitching point varies from leading edge to trailing edge. It is shown that as the pitching point moves aft of the mid-chord, a right half plane zero appears, causing the system to become non-minimum phase. This means that given a positive step in angle of attack, the lift coefficient will first dip negative, due to negative added-mass forces, before the circulatory forces take over and the lift relaxes to its positive steady state.

Extending previous work,[5,6] we have developed ROMs based on the indicial response linearized at non-zero angle of attack. Plotting the poles and zeros of the model as the base angle of attack is varied, we see a pair of complex poles march towards the imaginary axis, mimicking the Hopf bifurcation observed in the full Navier-Stokes equations. The models linearized at non-zero angle of attack are shown to capture

the dynamics of small amplitude motions, as shown in the Bode plot in Figure 9. It is not surprising that a ROM linearized at $\alpha = 15°$ performs significantly better than a model linearized at $\alpha = 0°$ for a rapid maneuver from 15° to 25°, shown in Figure 10. It is surprising how well the model performs, considering that a leading edge vortex forms and sheds during the maneuver.

It will be interesting to develop a model that interpolates between each of the ROMs for $\alpha \in [0, 25]$ for accurate performance over a larger range of angle of attack. Additionally, it will be important to extend these models to include the vortex shedding behavior observed at higher angles of attack.[18,19]

References

[1]Wagner, H., "Über die Entstehung des dynamischen Auftriebes von Tragflügeln," *Zeitschrift für Angewandte Mathematic und Mechanik*, Vol. 5, No. 1, 35 1925, pp. 17.

[2]Theodorsen, T., "General theory of aerodynamic instability and the mechanism of flutter," Tech. Rep. 496, NACA, 1935.

[3]Juang, J. and Pappa, R., "An eigensystem realization algorithm for modal parameter identification and model reduction," *J. Guid. Contr. dyn.*, Vol. 8, No. 5, 1985, pp. 620–627.

[4]Ma, Z., Ahuja, S., and Rowley, C., "Reduced order models for control of fluids using the Eigensystem Realization Algorithm," *Theor. Comput. Fluid. Dyn.*, 2009.

[5]Brunton, S. and Rowley, C., "Unsteady aerodynamic models for agile flight at low Reynolds numbers," *48th AIAA Aerospace Sciences Meeting and Exhibit*, 2010.

[6]Brunton, S. L. and Rowley, C. W., "Reduced order models for Wagner's indicial response," *in preparation*, 2010.

[7]Taira, K. and Colonius, T., "The immersed boundary method: a projection approach." *J. Comput. Phys.*, Vol. 225, No. 2, 2007, pp. 2118–2137.

[8]Colonius, T. and Taira, K., "A fast immersed boundary method using a nullspace approach and multi-domain far-field boundary conditions," *Comput. Methods Appl. Mech. Engrg.*, Vol. 197, 2008, pp. 2131–2146.

[9]Stengel, R., *Flight Dynamics*, Princeton University Press, 2004.

[10]Birch, J. and Dickinson, M., "Spanwise flow and the attachment of the leading-edge vortex on insect wings." *Nature*, Vol. 412, 2001, pp. 729–733.

[11]Sane, S., "The aerodynamics of insect flight." *J. Exp. Biol.*, Vol. 206, No. 23, 2003, pp. 4191–4208.

[12]Zbikowski, R., "On aerodynamic modelling of an insect-like flapping wing in hover for micro air vehicles," *Phil. Trans. R. Soc. Lond. A*, Vol. 360, 2002, pp. 273–290.

[13]Videler, J., Samhuis, E., and Povel, G., "Leading-edge vortex lifts swifts." *Science*, Vol. 306, 2004, pp. 1960–1962.

[14]Ahuja, S., Rowley, C., Kevrekidis, I., Wei, M., Colonius, T., and Tadmor, G., "Low-dimensional models for control of leading-edge vortices: Equilibria and linearized models." *AIAA Aerospace Sciences Meeting and Exhibit*, 2007.

[15]Ol, M., McAuliffe, B., Hanff, E., Scholz, U., and Kahler, C., "Comparison of laminar separation bubble measurements on a low Reynolds number airfoil in three facilities," *35th AIAA Fluid Dynamics Conference and Exhibit*, 2005.

[16]Kaplan, S., Altman, A., and Ol, M., "Wake vorticity measurements for low aspect ratio wings at low Reynolds number," *Journal of Aircraft*, Vol. 44, No. 1, 2007, pp. 241–251.

[17]Leishman, J. G., *Principles of Helicopter Aerodynamics*, Cambridge University Press, 2nd ed., 2006.

[18]Brunton, S., Rowley, C., Taira, K., Colonius, T., Collins, J., and Williams, D., "Unsteady aerodynamic forces on small-scale wings: experiments, simulations and models," *46th AIAA Aerospace Sciences Meeting and Exhibit*, 2008.

[19]Brunton, S. and Rowley, C., "Modeling the unsteady aerodynamic forces on small-scale wings," *47th AIAA Aerospace Sciences Meeting and Exhibit*, 2009.

[20]Goman, M. and Khabrov, A., "State-space representation of aerodynamic characteristics of an aircraft at high angles of attack." *J. Aircraft*, Vol. 31, No. 5, 1994, pp. 1109–1115.

[21]Magill, J., Bachmann, M., Rixon, G., and McManus, K., "Dynamic stall control using a model-based observer." *J. Aircraft*, Vol. 40, No. 2, 2003, pp. 355–362.

[22]Smith, A., *Vortex models for the control of stall.*, PhD thesis, Boston University, 2005.

[23]Noack, J., Afanasiev, K., Morzynski, M., Tadmor, G., and Thiele, F., "A hierarchy of low-dimensional models for the transient and post-transient cylinder wake." *J. Fluid Mech.*, Vol. 497, 2003, pp. 335–363.

[24]Rowley, C., "Model reduction for fluids using balanced proper orthogonal decomposition." *Int. J. Bifurcation Chaos*, Vol. 15, No. 3, 2005, pp. 997–1013.

[25]Eldredge, J. D., Wang, C., and OL, M. V., "A computational study of a canonical pitch-up, pitch-down wing maneuver," *39th AIAA Fluid Dynamics Conference*, June 2009.

[26]OL, M. V., Altman, A., Eldredge, J. D., Garmann, D. J., and Lian, Y., "Résumé of the AIAA FDTC Low Reynolds Number Discussion Group's Canaonical Cases," *48th AIAA Aerospace Sciences Meeting and Exhibit*, 2010.

[27]Chen, K. K., Colonius, T., and Taira, K., "The leading-edge vortex and quasisteady vortex shedding on an accelerating plate," *Physics of Fluids*, Vol. 22, No. 3, 2010.

[28]Koochesfahani, M. M., "Vortical patterns in the wake of an oscillating airfoil," *AIAA J.*, Vol. 27, 1989, pp. 1200–1205.

[29]Breuker, R. D., Abdalla, M., Milanese, A., and Marzocca, P., "Optimal Control of Aeroelastic Systems using Synthetic Jet Actuators," *49th AIAA/ASME/ASCE/AHS/ASC Structures, Structural Dynamics, and Materials Conference*, 2008.